BMC Genomics

RESEARCH Open Access

Genome-wide analysis of lncRNA m6A methylation in the mouse cortex after repetitive mild traumatic brain injury

Rongrong Zhong[1†], Chen Chen[2†], Yingao Zhang[2†], Conglin Wang[1], Meimei Li[1], Fanglian Chen[1], Lu Wang[1], Qiang Liu[1] and Ping Lei[1*]

Abstract

N6-methyladenosine (m6A), a prevalent post-transcriptional modification in eukaryotic RNA, plays a significant role in regulating sensory experiences, learning, and injury in the mammalian central nervous system. However, the pattern of lncRNA m6A methylation in the mouse cortex following repetitive mild traumatic brain injury (rmTBI) has not been explored. This study conducted a genome-wide analysis of lncRNA m6A methylation in the mouse cortex using methylated RNA immunoprecipitation sequencing (MeRIP-Seq). We identified 43,103 differentially methylated peaks. Notably, the expression of m6A peaks indicated altered methylation and expression levels of 423 lncRNAs after rmTBI. In addition, employing METTL3 inhibitor STM2457 demonstrated that functional METTL3 was essential for repairing neural damage caused by rmTBI and influenced spatial learning and memory in rmTBI-model mice. Thus, the m6A methylation pattern of lncRNA in the mouse cortex after rmTBI identifies METTL3 as a potential intervention target for epigenetic modification following such injuries.

Clinical trial number Not applicable.

Keywords Repetitive mild traumatic brain injury, LncRNA, m6A modification, Cerebral cortex, METTL3

Introduction

Traumatic brain injury (TBI) is a neurological disorder induced by external mechanical force, resulting in structural brain damage or functional alterations in cerebral physiology [1]. Globally, this condition affects approximately 10 million individuals annually through fatalities or hospitalizations with epidemiological projections suggesting that 50% of the population will sustain at least one TBI during their lifetime [2]. The persistent sequelae of TBI, including physical disabilities, cognitive deficits, and exorbitant healthcare expenditures—not only impair daily functioning but also impose a substantial socioeconomic burden. impairments that disrupt daily activities, along with high medical costs that create a substantial financial burden [3]. Clinically, TBI severity is stratified using the Glasgow Coma Scale (GCS) assessing ocular, motor, and verbal responses to classify injuries as mild TBI (mTBI), moderate, or severe [4]. Of particular concern is mTBI, which accounts for 70–90% of all TBI cases [5]. Although most mTBI patients achieve symptomatic resolution within 10 days post-injury, emerging evidence reveals that recurrent mTBI (rmTBI) induces cumulative

†Rongrong Zhong, Chen Chen and Yingao Zhang are co-first authors.

*Correspondence:
Ping Lei
leiping1974@163.com
[1]Deparment of Geriatrics, Tianjin Medical University General Hospital, No. 154, Anshan Road, Nanyingmen Street, Heping District, Tianjin 300052, China
[2]Department of Biochemistry and Molecular Biology, School of Basic Medical Sciences, Tianjin Medical University, Tianjin 300070, China

neuropathological effects. Specifically, repetitive injuries not only heighten vulnerability to subsequent trauma but also escalate risks for chronic cognitive decline and psychiatric disorders [6].

Long noncoding RNAs (lncRNAs), are non-coding molecular transcript RNAs that regulate the expression of approximately 70% of mammalian genes by interacting with DNA, RNA, and proteins [7]. Central to their functional plasticity is the dynamic N6-methyladenosine (m6A) modification - the most prevalent internal RNA modification in eukaryotes, orchestrated by methyltransferases (METTL3/METTL14 "writers"), demethylases (FTO/ALKBH5 "erasers"), and binding proteins (YTHDF "readers") [8]. Recent studies have shown that METTL3 drives TBI related neuroinflammation by stabilizing Basic Leucine Zipper Transcriptional Factor ATF-Like (BATF) mRNA in microglia [9]; FTO alleviates epilepsy susceptibility and brain damage after TBI by mediating epigenetic upregulation of Nuclear Receptor Subfamily 4 Group A Member 2 (NR4A2) [10]. Notably, gene expression profiling analysis has revealed abnormal alterations in lncRNA expression in the cerebral cortex and hippocampus following trauma in rat, mouse, and human brains [11]. LncRNAs are also implicated in a variety of pathophysiological processes after TBI and may play a key role in its complications, by regulating specific signaling pathways [12]. Additionally, certain lncRNAs have been identified as potential therapeutic targets for motor and cognitive recovery after TBI [13]. However, no study to date has interrogated how rmTBI-induced dysregulation of m6A regulators, particularly the METTL3/FTO axis coordinates lncRNA-mediated secondary neurodegeneration [14, 15]. Importantly, emerging evidence suggests that the functional regulation of lncRNAs may involve post-transcriptional modifications, particularly m6A [16]. In the context of TBI, m6A modification may act as an epigenetic switch controlling RNA metabolism during secondary brain injury progression [17]. While m6A's role in mRNA regulation during neural damage has been documented, its impact on lncRNA functionality in TBI pathophysiology remains completely unexplored, a critical knowledge gap given lncRNAs' established involvement in post-TBI complications [18]. As such, both lncRNAs and their m6A modifications hold promise as biomarkers for diagnosing, treating, and predicting outcomes in cases of rmTBI.

This study aimed to investigate the epigenetic modification of brain injury-associated RNA and their roles in neurogenesis following brain injury. In this study, we examined the impact of controlled cortical injury (CCI) on lncRNA m6A methylation profiles. Our investigation sought to explore a new dimension of epigenetic alterations in TBI through a genome-wide screen of transcriptional modifications in lncRNA m6A markers within the cerebral cortex. The objective was to uncover the potential role of lncRNA m6A-modified transcripts in the early physiological and pathological mechanisms of TBI. Additionally, we analyzed differential lncRNA expression following rmTBI. Through these analyses, we identified promising novel targets that may play a crucial role in developing further interventions for rmTBI.

Materials and methods

Reagents and chemicals

The METTL3 inhibitor STM2457 was obtained from MCE (MedChemExpress, USA), and TRIzol was purchased from Thermo (Thermo Fisher Scientific, USA). The m6A modification colorimetric quantification kit (P-9005) was sourced from EpiGentek. The primary antibody targeting m6A (#2435S) was acquired from Cell Signaling Technology (CST lnc., USA).

Animals

All animal testing protocols were approved by the Standard Medical Laboratory Animal Care Center. The procedures for this study were conducted in accordance with the guidelines of the Chinese Council on Animal Protection, and approved by the Institutional Animal Care and Use Committee of Tianjin Medical University General Hospital (IRB2022- DWFL-270). We made every effort to minimize animal suffering during the experiments. Male C57BL/6 mice (aged 8–10 weeks, each weighing approximately 23–25 g) were provided by Tianjin Medical University General Hospital. For the MeRIP-Seq experiment, a total of 18 mice was used, with nine mice randomly assigned to each group. Half of the mice were allocated to the rmTBI group, while the other half comprised the sham group (i.e., craniotomy only). RNA from three mice was pooled for each MeRIP-Seq sample, with each sample requiring at least 100 μg of RNA, including a minimum of 50 μg from each mouse's cortex. The behavioral testing experiment involved a total of 24 mice, with 6 randomly assigned to each of the following four group: sham operation group, rmTBI group, DMSO treatment group (rmTBI + DMSO), and STM2457 treatment group (rmTBI + STM2457). Using a stratified random sampling approach to minimize confounding variables such as body weight and baseline activity levels. Mice were first grouped by weight (23–25 g) and then assigned to each cohort using a computer-generated random number sequence (Microsoft Excel RAND function). This method ensured unbiased allocation without systematic differences between groups. Researchers performing behavioral tests were blinded to group assignments to further reduce selection bias. Each mouse was housed in the animal Experimental Center of Tianjin Medical University General Hospital under controlled conditions (temperature: 22–25 °C; relative humidity: 50%) with a normal

light/dark cycle of 12 h, and had free access to food and water (except overnight before surgery) for 1 week. Anesthesia was induced by intraperitoneal injection of 5% pentobarbital at a dose of 50 mg/kg.

The sample size was determined based on previous studies investigating m6A methylation dynamics in murine TBI models [19]. A power analysis ($\alpha = 0.05$, $\beta = 0.2$) using G*Power 3.1 indicated that $n = 6$ per group would detect a 2.10-3.63-fold difference in methylation levels with 80% power. To account for potential technical variability and attrition, we increased the sample size to $n = 9$ per group for MeRIP-Seq and $n = 6$ per group for behavioral testing.

Animal model of controlled cortical injury

The rmTBI animal model was established using the controlled cortical impingement (CCI) method, as previous described [20], with minor modifications. Briefly, metolazone (10 mg/kg) and ketamine (75 mg/kg) were administered via intraperitoneally injected. To maintain a constant body temperature of 37 °C, a heated blanket was utilized. A 4 mm diameter hole was drilled at an equidistant point between the lambda and bregma in the right hemisphere. The mice were then placed on a custom-designed CCI device (USA). The tip of a 3 mm impactor was placed at the center of the craniotomy, delivering a moderate injury at a speed of 3 m/s, with a residence time of 180 ms and a deformation depth of 1 mm. Mice exhibiting dural herniation or central occlusion damage was excluded from the study. After the surgery, the mice were monitored for 24 h, then fully anesthetized with 5% pentobarbital (50 mg/kg). Surgical collection of undamaged tissue surrounding the wound was performed, followed by cryopreservation at − 80 °C prior to RNA extraction.

RNA extraction and quantification of m6A in total RNA

In this study, total RNA was extracted from cortical tissues of both sham and rmTBI groups. To quantify m6A modifications, a colorimetry-based approach, similar to previously described visual assays, was employed [21]. Firstly, frozen tissue samples were pulverized using a chilled mortar and pestle until they were finely ground into fine powder. Each sample, with a fresh weight of 60 μg, was added to TRIzol and thoroughly mixed. Next, 200 μL of chloroform was added, followed by 15 s of vigorous shaking. The mixture was incubated at 25 °C for 5 min and then centrifuged at 13,000 rpm for 15 min at 4 °C. The supernatant was then mixed with an equal volume of 100% isopropanol, incubated at room temperature for 10 min, and centrifuged again. The resulting precipitate was washed with 1 mL of cold 75% ethanol. RNA pellets were air-dried for 5–10 min before being dissolved in 50 μL of RNase-free water. Negative controls and six m6A standard curve concentrations (ranging from 0.01 ng/μL to 0.5 ng/μL) were prepared. For the positive control, 200 ng of total RNA was used. The absolute m6A content in RNA was measured using an enzyme-linked immunosorbent assay (ELISA) on a SpectraMax + instrument.

MeRIP-Seq

To determine the level of m6A methylation in RNA, the MeRIP-Seq method was employed. This method uses an N6-methyladenine antibody to enrich hypermethylated RNA fragments, which are then subjected to high-throughput sequencing to detect m6A modifications across the entire transcriptome. Briefly, 20 μL of isolated 2× poly-A RNA was mixed with 250 μL of fragment buffer (10 mM ZnCl2, 10 mM Tris-HCl pH 7.0) to obtain a final volume of 270 μL. The sample was then denatured at 95 °C for 5–7 min using a thermal cycler. The reaction was halted by adding 0.5 M EDTA, and the sample was immediately placed on ice. The median size of the resulting RNA fragments was approximately 100 nt. Next, 20 μL of m6A-Dynabeads was rotated at 7 rpm (tail flip) at room temperature for 2 h. The m6A-Dynabead-RNA complex was resuspended in 500 μL of m6A binding buffer and incubated at room temperature for 3 min. Afterward, 125 μL of preheated elution buffer (50 °C) was added to the m6A-Dynabead complex and then incubated at 50 °C for 5 min. To purify m6A-positive RNA, 500 μL of acidic phenol-chloroform was added to the samples. For library construction, 100 ng of RNA was extracted from each sample (100 ng for both input and m6A-IP-positive post portion). All samples were sequenced using Illumina Hiseq X10 (SEQHEALTH, China).

Quantitative RT-PCR assay

For qRT-PCR analysis, total RNAs were extracted using RNA preparation kit (TransGen). The primers used for qRT-PCR are listed as follow:

Chrna10 Forward:
5'GCTCACAAGCTGTTTCGTGAC3'.
Chrna10 Reverse:
5'ACTTGGTTCCGTTCATCCATATC3'.
Efnb Forward: 5'TGTGGCTATGGTCGTGCTG3'.
Efnb Reverse: 5'TCTTCGGGTAGATCACCAAGC3'.
Trim21 Forward: 5'TGGTGGAGCCTATGAGTATCG3'.
Trim21 Reverse: 5'GGCACTCGGGACATGAACTG3'.

Bioinformatics analyses

Raw data in FASTQ format (raw read) was processed using Trimmatic software. The cleaned data was compared to the integrated reference genome with HISAT2 software (v2.1.0). ExomePeak software was employed to detect m6A-RIP-enriched regions (peaks), outputting

results in BED format. From the clean data, 250,000 reads were extracted, and BLASTn software was used for random alignment against the NT database (https://ftp.ncbi.nih.gov/blast/db), based on an e-value < 1e-10 and coverage > 80% indicating optimal alignment. Ribosomal RNA reads were discarded using SortMeRNA software, while the remaining clean reads were mapped to the reference genome using HISAT2 with default parameters, retaining unique reads of high mapping quality. Potential PCR duplicates were removed using Picard. Differential methylation peaks between the rmTBI and sham surgery group were analyzed using ExomPeak with criteria of fold-change ≥ 1.5 and $p < 0.05$. The quality of m6A seq data was assessed using the Trumpet R package. Peak calling for m6A-enriched areas in each m6A-immunoprecipitation sample was performed with MeTDiff, using the corresponding input sample as control. MeTDiff was configured with specific parameters (FRAGMENT_LENGTH = 200, PEAK_CUTOFF_PVALUE = 0.01, PEAK_CUTOFF_FDR = 0.05) for peak detection. Annotated peaks were determined by their intersection with gene architecture using ChIPseeker. Differential analysis was of m6A-Seq-identified RNA methylome differences was conducted in a case-control study, with differential peaks detected using MeTDiff under the certain parameters (FRAGMENT_LENGTH = 200, PEAK_CUTOFF_PVALUE = 0.01, DIFF_PEAK_CUTOFF_FDR = 0.05, PEAK_CUTOFF_FDR = 0.05). The differential peaks were afterwards annotated by ChIPseeker. To enrich the Gene Ontology peak and differential expression peak, the Gene Ontology (GO) and the Kyoto Encyclopedia of Genes and Genomes (KEGG) pathway enrichment analysis were employed. SPSS 25.0 software (IBM, USA) was utilized for the analysis, and Cytoscape version 3.7.2 software was used to build the m6A peak and lncRNA expression network.

Behavioral testing

To assess spatial learning and memory following rmTBI, two tests were conducted: the Modified Neurological Severity Score Y Maze Test (YMT) and the Morris Water Maze (MWM). The YMT used an arm which measured 30 cm in length, 8 cm in width, and 15 cm in height. Each mouse was placed at one end of the arm, and the number of arm alterations was recorded over a 5-minutes period. Working memory was calculated as the ratio of correct arm changes to the total number of arm entries, where correct alternation was defined as entering three different arms in successive selections. For the MWM test, a circular water tank with a diameter of 120 centimeters and a height of 30 centimeters was used. Each mouse's swimming activity was tracked, and the mice were trained to find a hidden platform within 60 s, with a total of 4 times. Afterwards, the delay, number of crossings, and time spent in the platform quadrant of crossing the platform area are officially recorded. After CCI, mice were intraperitoneally injected with the METTL3 inhibitor STM2457 (25 mg/kg) to inhibit METTL3 methyltransferase function.

Statistical analyses

Data were analyze using GraphPadPrism7.00 software. One-way ANOVA was employed to compare groups, with Tukey's post hoc test used to assess specific intergroup differences. A p-value of less than 0.05 was considered statistically significant and was denoted by an asterisk (*).

Results

Overall analysis of m6A MeRIP-Seq results

Our analysis indicated that MeRIP-Seq sample generated an average of 11.5 Gb of sequencing data, while the input sample generated 10.2 Gb. After removing the adaptor sequences, low-quality reads, and low-quality bases from both the 3′ and 5′ ends, the average amount of clean data was 9.6 Gb for the MeRIP-Seq sample and 10.2 Gb for the input sample. Notably, an average of 95.4% of the reads successfully mapped to the mouse genome. Clean reads that mapped to multiple locations in the mouse genome were eliminated (4.8%), leaving 95.2% as unique clean reads for further analysis.

Topological distribution of m6A peak profiles in the cerebral cortex after rmTBI

In total, 10,703 transcriptional genes were identified across all samples, among which there were 43,103 m6A peaks for which levels were upregulated and downregulated (Fig. 1A). Our analysis revealed that chromosomes 2, 7, and 1 harbored the highest number of m6A methylation sites, with 3413, 3180, and 3019 sites, respectively (Figure S1A). The number of m6A modified sites per gene ranged from 1 to 63, with approximately 99.6% of genes having either 1 or 2 methylation sites. The remaining 0.4% of genes consisted of 3 or more methylation sites. Notably, the gene Gm42416, located on chromosome 18, displayed the highest number of methylation sites, i.e., 63 sites.

Additionally, the distribution pattern of m6A methylation peaks was analyzed in relation to lncRNA gene structure. As per the GFF annotation of the reference genome, lncRNAs lacked coding sequences (CDSs) and other structural divisions typical of protein-coding genes. For our ncRNA analysis, we conducted a statistical distribution analysis of ncRNA regions as well as 1 kb upstream and downstream. Our findings suggest that the m6A peaks are predominantly located within the CDS region, with significant enrichment at both ends (i.e., near the start codon at the 5' end and the end codon at

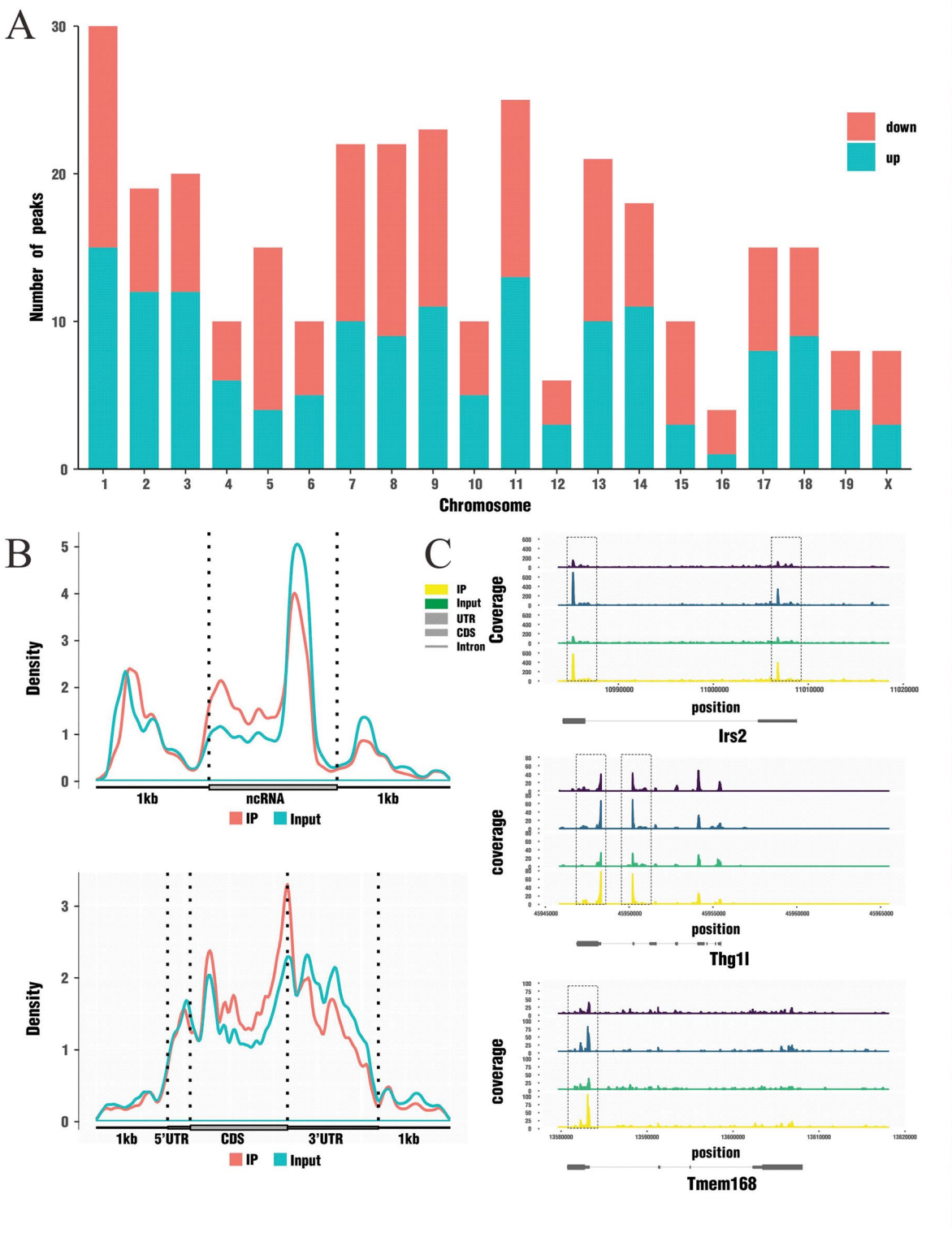

Fig. 1 Topological distribution of overall LncRNA m6A peaks. **A**, The distribution pattern of LncRNA m6A peaks in different chromosomes. **B**, The distribution patterns of m6A methylation peaks in gene structures of LncRNA. The peaks were mostly distributed on the exon region and there was a distinct enrichment peak at the 3′ terminate (near the stop codon) and an enrichment peak at the 5′ terminate (near the start codon). **C**, IGV plot shows directly the peaks in the genes of *Irs2*, *Thg1l* and *Tmem168*. The peak of *Irs2* was located at the 5′ UTR and 3′ UTR region, the peak of *Thg1l* was located at the CDS and 5′ UTR regions, and the peak of *Tmem168* was located at the 5′ UTR regions

the 3' end)(Figure S1B and S1C). Specifically, we noted that the number of reads in the input sample was higher in the CDS region than in the IP sample (Fig. 1B).

To further demonstrate the m6A methylation patterns, we selected three genes: Irs2, which showed peak signals in both the 5' UTR region and 3' UTR region; Thg1l, which displayed peaks in both the 5' UTR region and CDS region; and Tmem168, which exhibited peaks solely in the CDS region (Fig. 1C). Furthermore, Table 1 lists the top 20 m6A peaks that exhibited the most significant changes in the cerebral cortex following rmTBI.

m6A methylation is significantly changed after rmTBI

The levels of methylation in the cortex were compared between rmTBI and sham groups of mice. Our findings revealed an average of 21,990 peaks in the rmTBI group, compared to 21,882 peaks in the sham group (Fig. 2A). The average logarithmic enrichment multiple was 4.27 for the rmTBI group and 4.12 for the sham operation group (Fig. 2B), showing a remarkable difference when compared to the input sample. Further, the mean peak length of the TBI group was 3,315.03 bp, while the sham group had a mean peak length of 3,720.62 bp (Fig. 2C).

Based on the consensus, 313 peaks with significant changes were indicated ($p < 0.01$ $FDR < 0.05$), with 154 peaks significantly upregulated and 159 peaks significantly downregulated (Fig. 3A). Table 1 lists the initial 20 lncRNAs showing differential methylation, while spikes were observed in 1,580 out of 4,900 genes. All peaks exhibited an average logarithmic-enrichment multiple of 2.42 (Fig. 3B). The average length of each peak was found to be 4,358.7 bp (Fig. 3C). A clear representation of the distribution of p-values among each peak was depicted in Fig. 3D. The peaks with significant changes were primarily located in CDSs (39.55%), exons (7.4%), the 3′ UTR (45.02%), and the 5′ UTR (8.04%; Fig. 4A). Notably, peaks were associated with significant changes in multiple genes: 556 peaks were distributed in the CDS and 3′ UTR region, 532 peaks in the CDS and intron region, and 495 peaks soled in the CDS region (Fig. 4B). Three representative genes with significant changes in their peaks are shown in shown in Fig. 4C-E. After rmTBI, the lncRNA m6A levels of *Chrna10*, *Efnb1*, and *Trim21* increased by 3.13-, 1.54-, and 2.14-fold, respectively. These changes in lncRNA expression were confirmed using quantitative RT-PCR (Fig. 4F).

GO and KEGG analysis revealing the biological information regulated by m6A methylation

GO analysis indicated that m6A methylation was associated with three parts of biological information. In term of molecular functions, significant associations included RNA binding, poly(A) RNA binding. For cell components, relevant terms encompassed synapse part, synapse, postsynaptic specialization, postsynaptic density, postsynapse, neuron projection, neuron part, excitatory synapse, and dendrite. Regarding biological process, key associations were found with trans-synaptic signaling, synaptic signaling, neuron projection development, neuron projection morphogenesis, nervous system development, chemical synaptic transmission, cell projection

Table 1 The top 20 m6A peaks that were found to exhibit the most significant changes in the cerebral cortex after rmTBI

GENE	Chr	Start	End	Length	Strand	logFC	Pvalue
Slc38a11	2	65,316,548	65,316,668	121	-	7.463616	0.032665
Ddx60	8	61,994,442	61,994,503	62	+	6.954337	0.00044
BC037032	15	4,022,567	4,022,628	62	-	6.335118	0.005529
Eif2ak2	17	78,853,102	78,853,163	62	-	5.310275	0.006045
Gm17021	9	1.24E + 08	1.24E + 08	151	-	5.018454	0.017165
Gm26621	15	68,335,460	68,335,521	62	-	4.26937	0.036343
Kif20b	19	34,950,013	34,950,074	62	+	4.053933	0.002129
Gm44284	6	42,329,041	42,329,102	62	-	4.035709	0.038429
Tnfrsf1b	4	1.45E + 08	1.45E + 08	181	-	4.030157	0.003654
Ybey	10	76,462,710	76,462,831	122	-	3.944858	0.042984
Htr4	18	62,464,488	62,464,579	92	+	-3.45121	0.047353
Fam161a	11	23,030,488	23,030,579	92	+	-3.55383	0.01625
Espnl	1	91,346,720	91,346,900	181	+	-3.62569	0.003917
Hist1h2be	13	23,585,257	23,585,406	150	-	-3.9272	0.031584
Sh3tc1	5	35,729,006	35,729,097	92	-	-4.07837	0.007384
Upf3a	8	13,798,894	13,799,044	151	+	-4.13652	0.010565
Pou6f2	13	18,122,898	18,122,959	62	-	-4.15675	0.042434
Chd1	17	15,770,575	15,770,725	151	+	-4.37316	0.017218
Dmgdh	13	93,752,292	93,752,383	92	+	-4.48897	0.0211
Kbtbd2	6	56,778,361	56,778,422	62	-	-4.70938	0.021154

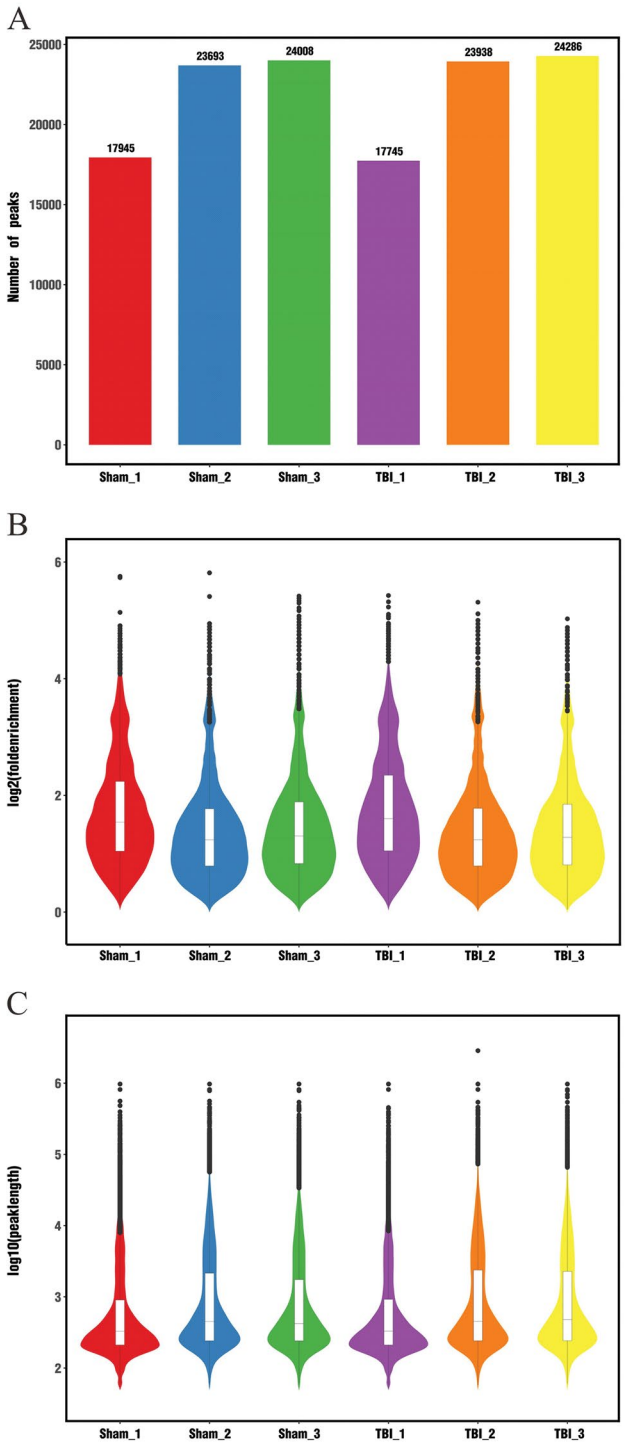

Fig. 2 Number of peaks, fold enrichment of peaks and length of peaks in two groups after rmTBI. **A**, The peak number of two groups. An average of 21,990 peaks in the rmTBI group and an average of 21,882 peaks in the sham group were identified. **B**, The enrichment of two groups. The average logarithmic fold-enrichment of TBI group was 4.27, and the average logarithmic fold-enrichment of sham group was 4.12. **C**, The peak length of two groups. The average peak length of rmTBI group was 3315.03 bp, and the average peak length of sham group was 3720.62 bp

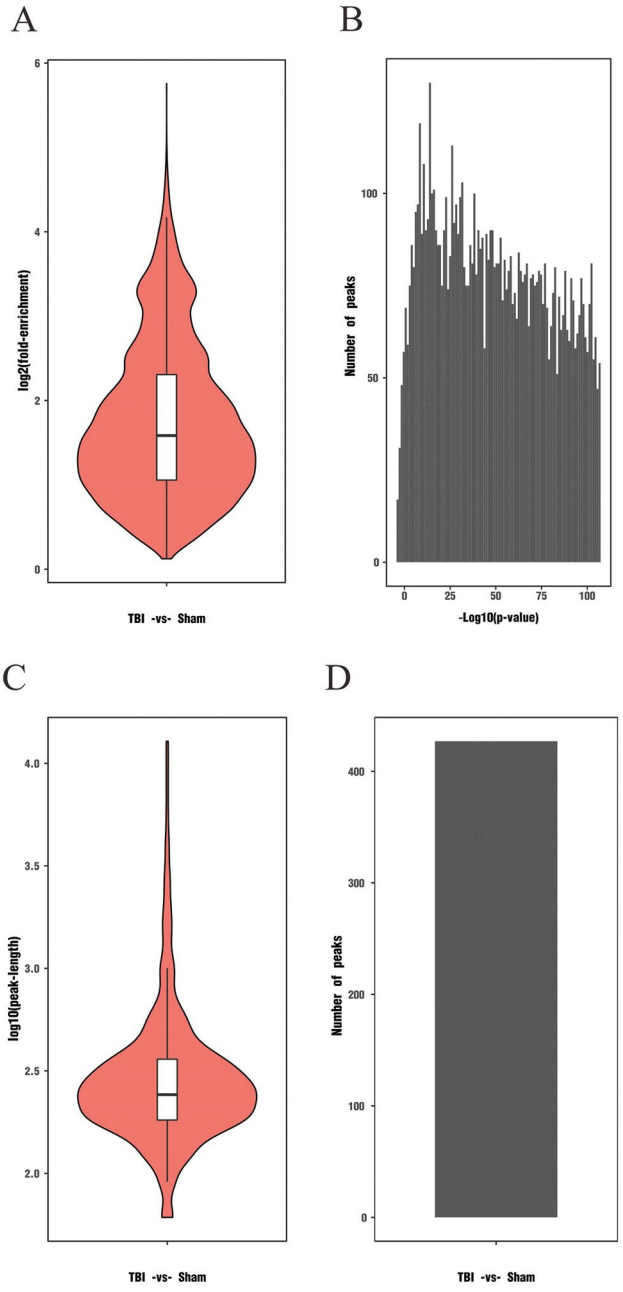

Fig. 3 Peak number, fold enrichment, peak length and *p*-value in the rmTBI and Sham groups. **A**, A total of 313 significantly changed peaks were identified ($p < 0.01$, FDR < 0.05). **B**, The average logarithmic fold-enrichment of the peaks were 2.42. **C**, The average length of each peak was 3.64 ($\log_{10}$). **D**, The distribution of *p*-value of all peaks

morphogenesis, cell part morphogenesis, and anterograde trans-synaptic signaling (Fig. 5A).

KEGG analysis further identified genes with significant changes in m6A methylation levels, which were primarily linked to various pathways, including the Wnt signaling pathway, thyroid hormone signaling pathway, spliceosome, Rap1 signaling pathway, pathways in cancer, oxytocin signaling pathway, nicotine addiction, neurotrophin

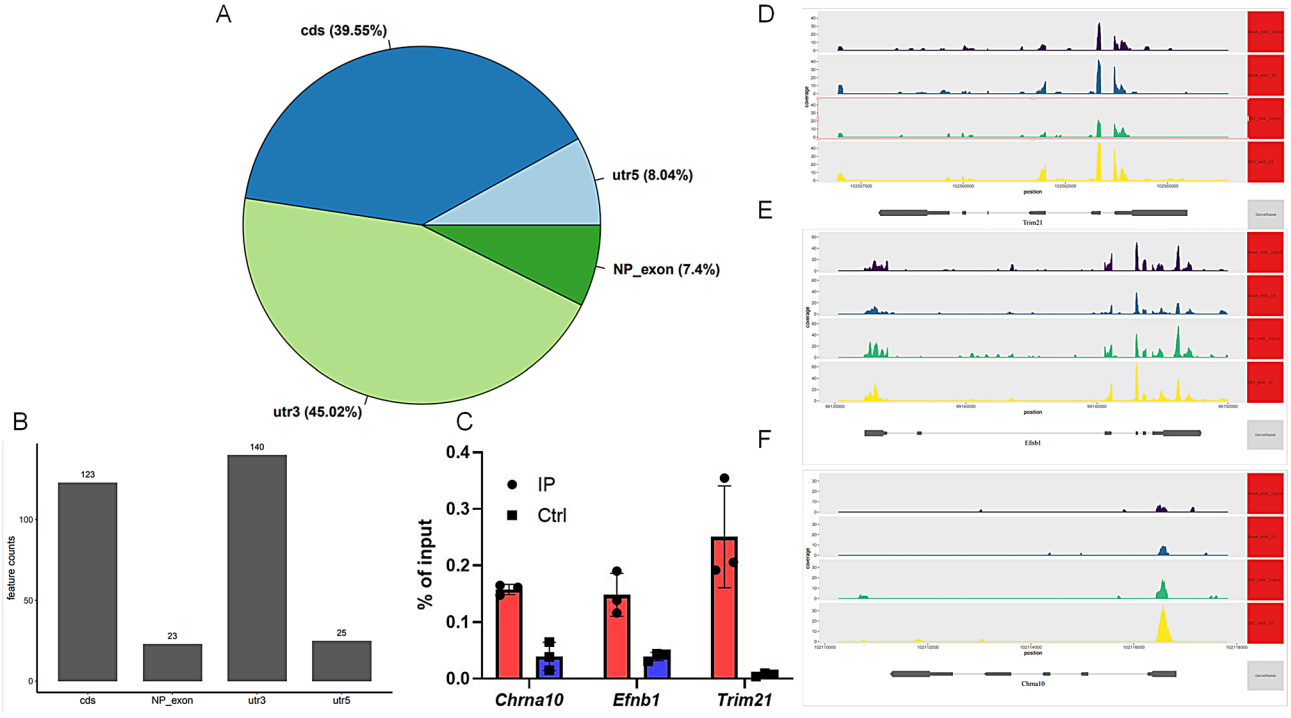

Fig. 4 The distribution of significantly changed peaks after rmTBI. **A**, Sector graph shows the ratio of peaks in each region. The peaks with significant changes were mainly distributed in the exon (7.4%), CDS (39.55%), 3′ UTR (45.02%), and 5′ UTR (8.04%) and only 0.02% were found in the intergenic region. **B**, Showing the exact distribution pattern of significantly changed peaks after rmTBI. There were 123 peaks distributed in the CDS and 140 peaks in the 3′ UTR regions, 23 peaks in exon regions, and 25 peaks in the 5′ UTR region. **C**, **D** and **E**, Three representative genes with significantly changed peaks. The LncRNA m6A level of *Chrna10*, *Efnb1*, and *Trim21* were significantly up-regulated after TBI by 3.13 fold, 1.54 fold, 2.14 fold, respectively. **F**, Changes in lncRNA expression confirmed by using quantitative RT-PCR

signaling pathway, MAPK signaling pathway, long-term potentiation, Hippo signaling pathway, glutamatergic synapse, gap junction, ErbB signaling pathway, endocrine resistance, EGFR tyrosine kinase inhibitor resistance, circadian entrainment, calcium signaling pathway, axon guidance, and adrenergic signaling in cardiomyocytes, among others (Fig. 5B). Additionally, the peak m6A was observed to exhibit a typical RRACH motif, where R represents A or G, and H represents A, C, or U (Figure S2B).

Gene expression profiles after rmTBI

Significantly different expressed genes were identified through hierarchical clustering, which revealed distinct gene expression patterns between the two groups. Specifically, 277 lncRNAs showed increased expression, while 146 lncRNAs showed decreased expression ($p < 0.05$, $\log_2 FC > 1$) in the mouse cerebral cortex after TBI (Fig. 6A). The top 20 differentially changed lncRNAs were organized in Table 1. The encoding potential assessment tool was utilized to assess the encoding capability of the novel transcript, and a heatmap displayed the relative expression level of the three TBI IPs (Fig. 6B). Compared to the sham group, 1,108 genes were differentially expressed (fold-change ≥ 1.5 and $p < 0.05$), with 931 genes upregulated and 177 downregulated. The volcano plot (Fig. 6C) showed the significantly upregulated and downregulated lncRNAs following TBI. The top six most significantly upregulated genes (*Klf4*, *Cspg4*, *Jmy*, *Com21*, *Maml3*, *Ephb4*) and the top six downregulated genes (*Zfpm1*, *Mrpl10*, *Ccdc40*, *Usp40*, *Nifk*, *Aak1*) are highlighted in the volcano plot.

METTL3 Inhibition attenuates the signs of rmTBI

Our aim was to investigate the impact of METTL3 inhibition on cognitive ability (Figure S2A), evaluated using the Y-maze test and MWM test in sham and rmTBI-model mice. The Y-maze test evaluates short-term working memory, and we observed a decline in the rate of spontaneous alternations in the rmTBI group compared to the sham group. However, treatment with STM2457 significantly increased the rate of spontaneous alternations, thereby improving learning and memory in rmTBI-model mice (Fig. 7A-G).

During the MWM test, which assesses locomotor and exploratory behavior, the rmTBI group showed a longer escape latency during the training trials (at day 3–5) compared to the sham group (Fig. 7C). In the probe trial (day 5), the rmTBI group spent less time in the target quadrant and made fewer platform crossings (Fig. 7E and F). However, STM2457 treatment positively influenced

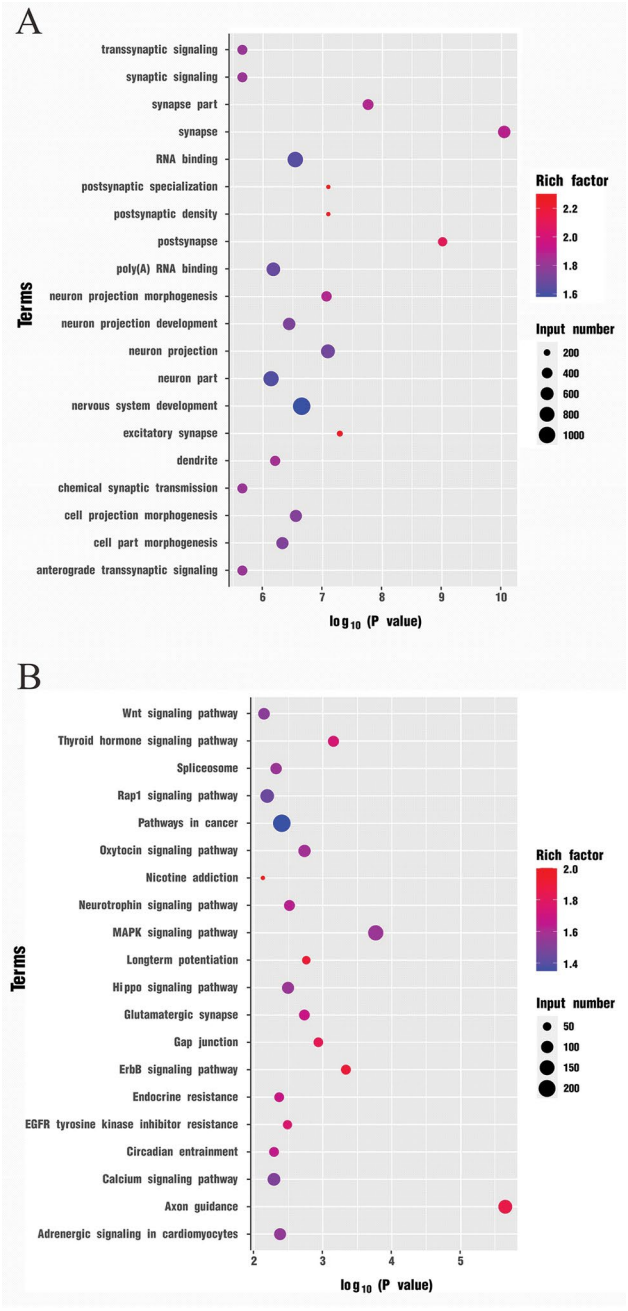

Fig. 5 GO and KEGG analyses revealed the biological information behind LncRNA m6A methylation. **A**, The top 20 enriched GO terms of the LncRNA m6A peaks. **B**, The top 20 enriched KEGG pathways of LncRNA m6A peaks

spatial learning and memory by decreasing the escape latency and increasing the number of platform crossings, resulting in more time spent in the target quadrant.

These observations indicated that METTL3 inhibition in rmTBI-model mice did not impact motor functions but improved learning and memory deficits induced by rmTBI (Fig. 7E-G). Taken together, our findings emphasize the significance of METTL3 inhibition in rmTBI progression. Furthermore, cognitive impairment following rmTBI can be mitigated with STM2457 administration, as evidenced by the results of YMT and MWM tests.

Discussion

Just as histone and DNA undergo chemical modifications, RNA also features reversible chemical modifications. Among them, m6A methylation is the most common new RNA modification, closely linked to the occurrence and progression of nurmerous diseases [22]. In recent years, increasing attention has been directed toward m6A changes in neurological diseases. It has been found that axonal injury leads to elevated m6A levels [23], which in turn promote the expression of many genes related to regeneration in adult dorsal root ganglion. Comprehensive investigations of RNA m6A transcriptome in the mouse cerebral cortex during behavioral training suggest that m6A methylation may be implicated in memory consolidation. Additionally, mRNA and lncRNA modified by m6A methylation have been observed in patients with neurological disorders. The methyltransferase complex, which includes METTL3, METTL14, and WTAP, as well as demethylation enzymes like FTO and ALKBH5, dynamically regulate m6A modification. METTL3 is a crucial RNA N6-adenosine methyltransferase, and its downregulation has been shown to enhance cell proliferation and migration while inducing G0/G1 cell cycle arrest [24]. Increasing evidences suggest that METTL3 plays a significant role in nervous system functions, with m6A methylation in the adult mouse brain being regulated by stressed regions and at specific times. Notably, knocking out of METTL3 in the mouse cerebellum leaded to increased apoptosis in the outer granulosa layer of the newborn cerebellum [25]. This reduction in m6A modification prolongs RNA half-life and disrupts splicing events, resulting in maltranscription of genes and premature death of cerebellar granulosa cells. Moreover, METTL3 silencing has been linked to impaired spatial learning and memory in the hippocampus.

Previous studies have demonstrated that the expression of METTL3 decreases in the hippocampus shortly after TBI via qPCR detection. Immunostaining confirmed that METTL3 was predominantly expressed in neurons, suggesting that impaired cognitive function may be associated with abnormal regulation of METTL3 [26]. Research has also indicated decreased expression of METTL14 and FTO in mice with repeated TBI. Specifically, METTL14 interacts with METTL3 to form a methyltransferase complex, facilitating RNA m6A methylation [27]. The demethylase FTO can mediate the demethylation of RNA m6A. The downregulation of both METTL14 and FTO following rmTBI resulted in an increase in 154 methylation peaks and a decrease in 159 methylation peaks. Inhibition of FTO can exacerbate

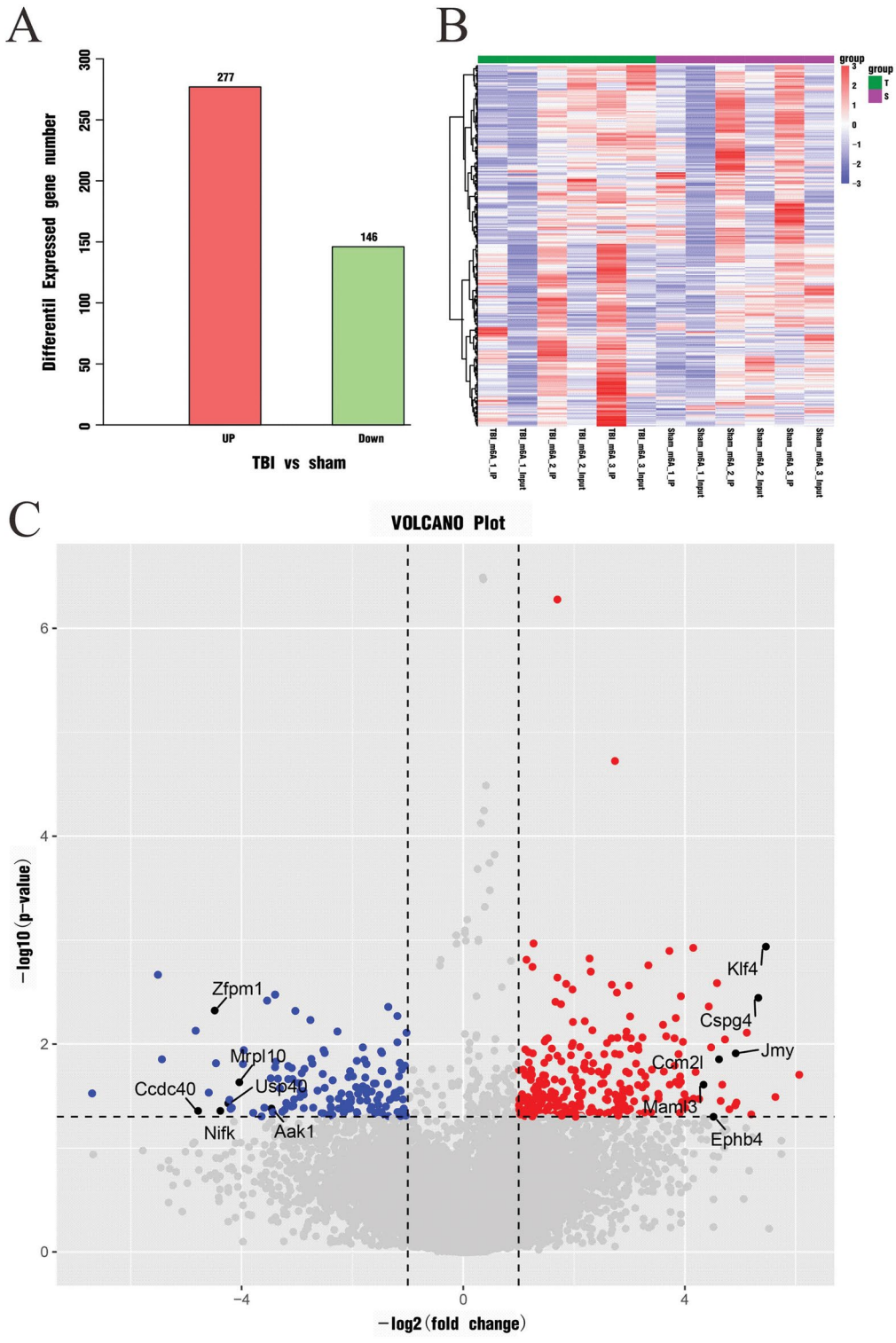

Fig. 6 LncRNA changes after rmTBI. **A**, The expression level of LncRNA after rmTBI. A total of 277 LncRNA expression increased and 146 LncRNA expression decreased ($p < 0.05$, $\log_2 FC > 1$) in mice cerebral cortex after rmTBI. **B**, Heat map shows the relative expression level of the three rmTBI IP and the three sham IP. **C**, Volcano plot shows the significantly up-regulated and down-regulated LncRNA after rmTBI

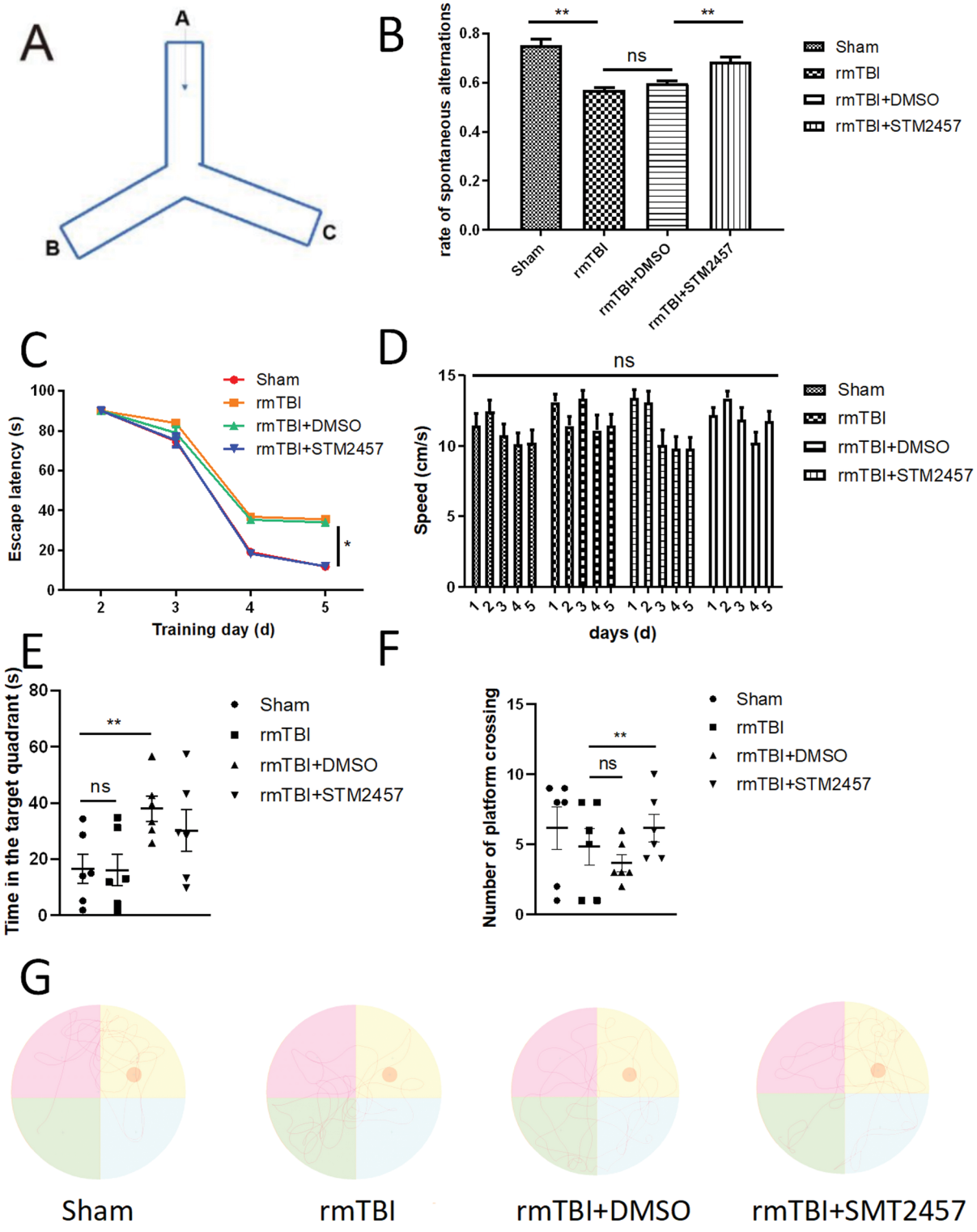

Fig. 7 METTL3 inhibition in improving the cognition in a mouse model of rmTBI. **A**, Experimental design of the YMT for the sham and rmTBI mice. **B**, The spatial working memory of the sham or rmTBI mice in the YMT. Alternations were counted as the percentage of "correct" alternation/total entries. "Correct" alternation means entry into all 3 arms on consecutive choices. **C–F**, The sham or rmTBI mice were trained and learned to find a hidden platform over 5 consecutive days. The escape latencies of the sham or rmTBI mice in the MWM task on training days were recorded (**C**). On Day 5, probe trials were performed with the platform absent, and the swim speed (**D**), the time in target quadrant (**E**), and number of platform area crossings (**F**) were assessed. **G**, Representative MWM swim plots (G) for the sham and rmTBI mice on Day 5. All data were presented as the mean ± SEM. *$p < 0.05$, **$p < 0.01$, "ns" means no significance ($p > 0.05$) ($n = 6$)

nerve injury [28], implying that increased FTO expression and enhanced activity may accelerate nerve repair after TBI [29]. Given that METTL14 expression declined after TBI, METTL14 inhibitors should be used to confirm these conclusions. The distribution of m6A peaks across various methylation events in TBI was found to be predominantly located in the 3' UTR near stop codons and 5' UTR near start codons, consistent with previous studies in human and mouse models. Notably, m6A modification is extensively enriched in the 3' UTR region of lncRNA (45.02%), particularly at the initiation of the final exon, where it exhibits a dramatic increase (up to 6-fold). Overall, these findings suggest that m6A modification may play a pivotal role in the development of the nervous system as well as in the preservation of memory and learning abilities.

In the context of rmTBI, m6A modification of lncRNAs is increasingly recognized as a crucial regulatory mechanism in neural stress responses and repair processes. Most m6A modifications are found in mRNA exons, with some also present in lncRNA [30]. Although direct studies on m6A-modified lncRNAs in rmTBI are still limited, several lncRNAs—such as VLDLR-AS1, MALAT1, H19, and ZFAS1—have been reported to undergo expression changes following TBI and play key roles in neural function regulation. Specifically, VLDLR-AS1 is significantly downregulated in the serum of veterans with rmTBI and is associated with depressive symptoms, indicating its possible involvement in cognitive regulation via stress-related pathways [31]. MALAT1, derived from adipose stem cell–secreted exosomes, activates regenerative pathways and modulates inflammation in a mouse TBI model, thereby improving neurological function [32]. Knockdown of H19 has been shown to activate the Nrf2/HO-1 antioxidant pathway, attenuating inflammation and oxidative stress, and promoting neurorepair [33]. Similarly, silencing ZFAS1 reduces cerebral edema and neuronal apoptosis after TBI [34]. These lncRNAs have been confirmed in other studies to possess m6A modification sites. m6A is thought to influence their stability, splicing, and interactions with RNA-binding proteins, thereby amplifying their functional impact during pathological processes. These lncRNAs are also known to be major targets of m6A modification, suggesting a potential link.

This study is the first to report the distribution of lncRNA m6A in the cerebral cortex of mice following TBI. We used m6A-RIP-seq for a whole-genome analysis of m6A-labeled lncRNAs at 6 h following TBI in mice. In total, 313 m6A peaks were significantly differentially expressed, with 154 peaks upregulated and 159 downregulated. Moreover, we conducted analyses of GO and KEGG pathway to infer the potential impact of transcript changes resulting from m6A modifications. These results, based on a mouse model of TBI, may align meaningfully with the epigenetic changes associated with m6A in human studies [22]. During brain development, the central nervous system relies on various substrates, such as glucose, amino acids, fatty acids, and vitamins, for energy supply, protein synthesis, hormone secretion, synaptic formations, and the metabolism required for all cellular processes. These processes are crucial for maintaining intracellular and intracellular ion concentrations, neurotransmitter release and uptake, and myelin formation. Metabolic changes resulting from brain injury can lead to long-term cognitive and neurological dysfunction. Notably, our GO analysis results demonstrated that m6A-modified transcript changes primarily affected the regulation of metabolic and cell metabolic processes, highlighting the significant role of m6A modification in the metabolic changes that follow TBI. Given that rmTBI can induce persistent brain metabolic disorders, such as post-traumatic epilepsy, targeting m6A modification may represent a valuable clinical strategy. Nevertheless, further research is warranted to unveil the precise mechanisms underlying this phenomenon. In light of the potential involvement of m6A modification in post-TBI pathophysiological processes, modulating m6A levels may offer a promising and novel therapeutic approach.

The methylation levels of m6A, closely linked the pathophysiological process of TBI, exhibits significant alterations. Autosomal recessive cerebellar atrophy, often associated with inactivation mutations and early-onset symptoms, has been implicated in neuronal survival pathways. Notably, whole exome sequencing has identified Thg1l as a key player in cerebellar atrophy. It is well established that THG1L protein modulates mitochondrial fusion via interactions with MFN2, thereby promoting cellular respiration by enhancing oxidative phosphorylation and electron transport chain activity, which stimulates mitochondrial activity. These findings suggest a pivotal role for THG1L in regulating MFN2 activity and indicate its potential significance in brain injury, aligning with our observations. Neuroinflammation contributes to insulin resistance in the brain, processes that are strongly linked to neurodegenerative diseases, including brain damage [35]. Potential mechanisms include insulin receptor substrate (IRS) and serine phosphorylation or insulin receptor (IR) mismatch. In models of neuroinflammation, a notable reduction in the expression of both mRNA and IRS2 protein has been observed, along with a significant increase in tumor necrosis factor-α (TNF-α) and amyloid precursor protein (APP) levels within the hippocampus. Conversely, there was a decrease in the expression of brain-derived neurotrophic factor (BDNF), leading to reductions in neurogenesis. Neuroinflammation may variable affect the expression of IRS1 and IRS2 in the hippocampus [36]; however, its specific role in rmTBI remains unknown.

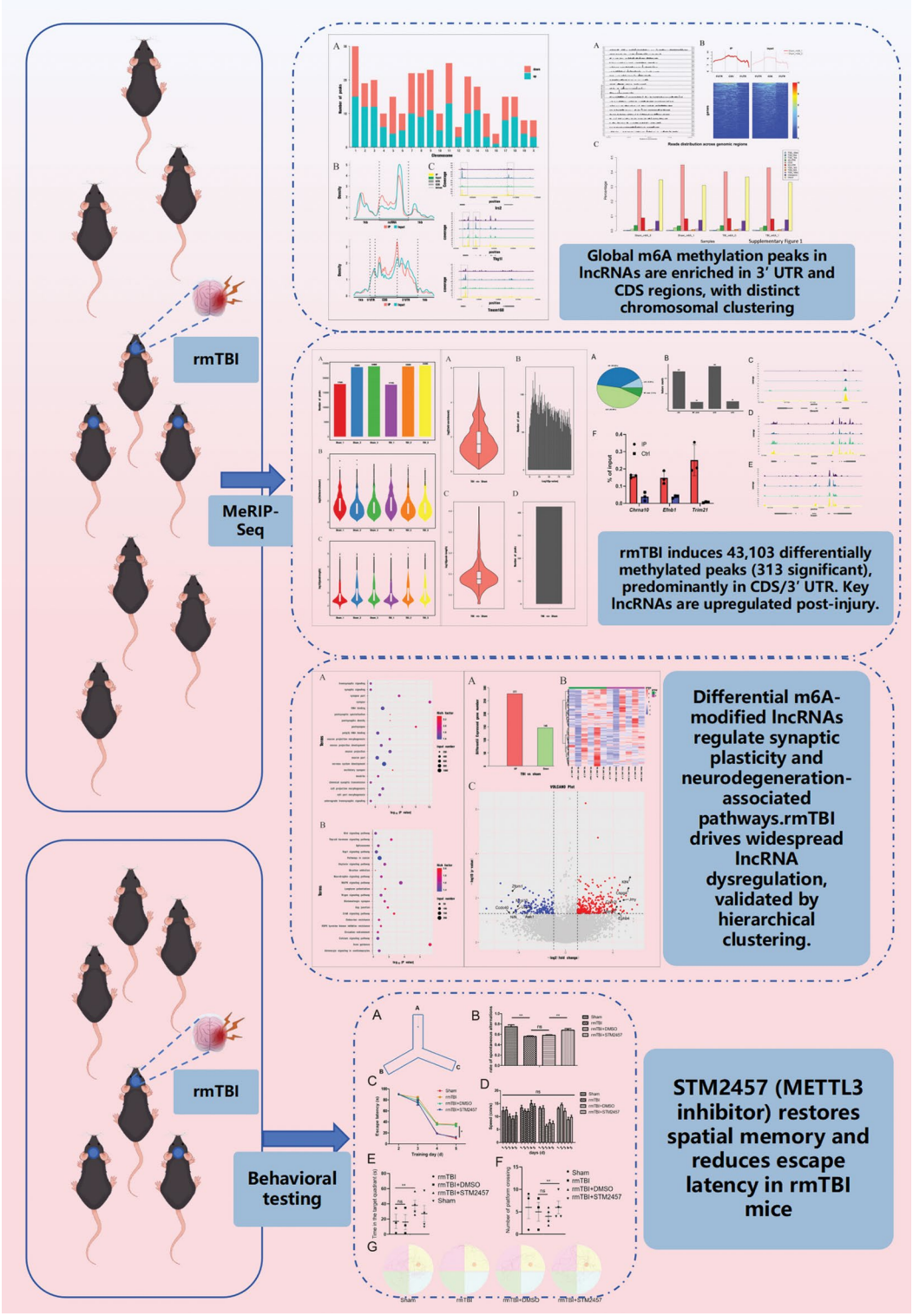

Fig. 8 METTL3-mediated lncRNA m6A methylation drives cognitive recovery after repetitive mild traumatic brain injury. This study investigates the role of METTL3-mediated m6A methylation in lncRNAs following repetitive mild traumatic brain injury (rmTBI) in mice. Using methylated RNA immunoprecipitation sequencing (MeRIP-Seq), we identified 43,103 differentially methylated peaks, with 313 showing significant changes, predominantly localized in coding sequences (CDS) and 3′ untranslated regions (3′ UTR). Key lncRNAsexhibited marked upregulation, validated by qRT-PCR. Functional enrichment analysis linked these modifications to synaptic signaling, neuronal development, and pathways such as Wnt and glutamatergic synapse. Behavioral assays demonstrated that METTL3 inhibition via STM2457 improved spatial memory in rmTBI mice, evidenced by increased spontaneous alternations in the Y-maze and reduced escape latency in the Morris water maze. Integrated expression profiling revealed 277 upregulated and 146 downregulated lncRNAs post-injury

TMEM168 has been associated with the development of human glioma, where *TMEM168* mRNA levels are upregulated in glioma patients, consistent with the results of this study. This enhanced expression of *TMEM168* correlates with shorter survival time [37]. Therefore, it is speculated that *TMEM168* might also serve be a target for treating human brain injury. These genes may represent key genes that disrupt the epigenetic regulation of TBI. However, the precise protein levels associated with these m6A-methylated lncRNAs cannot be predicted and warrant further investigation.

The m6A modification affects various aspects of RNA processing, including maturation, decay, selective polyadenylation, splicing, and translation of proteins in the cytoplasm. The diverse functions of m6A are largely attributed to its associated binding proteins, which can either promote or inhibit protein translation. For instance, YTHDF1 and YTHDF3 are known to promote protein translation, whereas YTHDF2 as an inhibitor. By analyzing m6A-RIP-seq data, our study identified differentially expressed transcripts that were either hypermethylated or hypomethylated, shedding light on the function of m6A readers in TBI.

Our study demonstrated that inhibiting METTL3 reduces m6A modification of lncRNA and alleviates symptoms of rmTBI. METTL3 has been associated with hippocampal memory functions, while FTO is involved in various physiological and pathological functions within brain tissue. Additionally, METTL14, another m6A RNA methyltransferase, plays a crucial role in the transcriptional regulation of striatal functions and learning. Dysregulated methylation of RNA has been linked to TBI, particularly concerning cerebellar and neural development. Our findings highlight the importance of regulating m6A modification in the context of rmTBI and may inform future research aimed at improving outcomes for affected patients.

While our study establishes METTL3-mediated m6A modification of lncRNAs as a critical regulator of post-TBI recovery, several limitations warrant consideration. First, the behavioral cohort may lack statistical power to detect subtle cognitive improvements due to high inter-individual variability in rmTBI models. Second, the CCI model replicates focal cortical injury but poorly mimics human diffuse axonal injury patterns, and the 14-day observation window precludes assessment of chronic neurodegeneration (>6 months post-TBI), during which m6A dynamics may shift. Third, the exclusive use of male mice, although controlling hormonal variability, overlooks estrogen's modulation of FTO activity, potentially inflating therapeutic effect sizes in female populations. Future studies should prioritize temporally controlled genetic models to resolve cell-type-specific methylation effects, validate m6A biomarkers in cerebrospinal fluid exosomes for chronic neurodegeneration monitoring, and refine targeted RNA modification tools to address current technical constraints.

In summary, our study suggests that inhibiting METTL3 expression in the cerebral cortex of mice following rmTBI can effectively alleviate cognitive impairment from brain injury. A genome-wide analysis and subsequent bioinformatics analysis of m6A-modified transcripts revealed the potential function of these changed m6A-transcripts. Additionally, analysis of m6A-RIP-seq data identified differentially expressed hypermethylated and hypomethylated mRNA peaks. Several clinical trials targeting the early stage of rmTBI treatment are currently underway. Our findings may offer new options for developing treatment strategies for rmTBI (Fig. 8).

Abbreviations

CCI	Controlled Cortical Injury
m6A	N6-methyladenosine
MeRIP-Seq	Methylated RNA Immunoprecipitation Sequencing
qRT-PCR	Quantitative Reverse Transcription Polymerase Chain Reaction
TBI	Traumatic Brain Injury

Supplementary Information

The online version contains supplementary material available at https://doi.org/10.1186/s12864-025-11696-6.

Supplementary Material 1: Supplementary Figure 1. Topological distribution of long noncoding RNA (lncRNA) N6-methyladenosine (m6A) peaks. A, Distribution pattern of m6A peaks in different chromosomes. B, Distribution pattern of m6A peaks in different genes of the two groups. C, Distribution pattern of m6A peaks in different gene regions. Supplementary Figure 2. Schematic illustration of the timeline of the experiments and the motif analysis. A, Timeline of the experiments. B, Peak N6-methyladenosine (m6A) motif analysis.

Acknowledgements

Not Applicable.

Author contributions

RRZ, CC and YAZ wrote the main manuscript. CLW, MML and FLC prepared the data collection. LW and QL prepared figures and table. RRZ, CC, YAZ and PL analyse and interpret of results. All authors reviewed the results and approved the final version of the manuscript. All authors would be informed each step of manuscript processing including submission, revision, revision reminder, etc.

Funding

This research was funded by Grants 22HHXBSS00047 from Haihe Laboratory of Cell Ecosystem Innovation Fund. Grants 82072166,82071394 from the National Natural Science Foundation of China. Grants 20YFZCSY00030 from the Tianjin Science and Technology Program. Grants TJWJ2021QN005 from the Science and Technology Project of Tianjin Municipal Health Commission. Grants 82102318 from the National Natural Science Foundation of China.

Data availability

The datasets generated and analysed during the current study are available in the Gene Expression Omnibus (GEO) database, with accession numbers of GSE287356.

Declarations

Ethics approval and consent to participate

All animal testing protocols were approved by the Standard Medical Laboratory Animal Care Center. The procedures for this study were conducted

in accordance with the guidelines of the Chinese Council on Animal Protection, and approved by the Institutional Animal Care and Use Committee of Tianjin Medical University General Hospital (IRB2022- DWFL-270).

Consent for publication
Not Applicable.

Competing interests
The authors declare no competing interests.

Received: 14 December 2024 / Accepted: 9 May 2025
Published online: 20 May 2025

References

1. Bergquist TF, Kew CL, Wisinger AM. Traumatic brain injury. Neurol Clin. 2024;42(4):863–74. https://doi.org/10.1016/j.ncl.2024.05.011.
2. Cáceres E, Olivella JC, Di Napoli M, Raihane AS, Divani AA. Immune response in traumatic brain injury. Curr Neurol Neurosci Rep. 2024;24(12):593–609. https://doi.org/10.1007/s11910-024-01382-7.
3. Malhotra AK, Jaffe RH, Shakil H, et al. Unemployment and personal income loss after traumatic brain injury. JAMA Surg. 2024;159(12):1415–22. https://doi.org/10.1001/jamasurg.2024.4285.
4. Leontyev D, Pulliam AN, Ma X, Gaul DA, LaPlaca MC, Fernández FM. Spatial lipidomics maps brain alterations associated with mild traumatic brain injury. Front Chem. 2024;12:1394064. https://doi.org/10.3389/fchem.2024.1394064. Published 2024 May 30.
5. MacLean MA, Muradov JH, Greene R, et al. Memantine inhibits cortical spreading depolarization and improves neurovascular function following repetitive traumatic brain injury. Sci Adv. 2023;9(50):eadj2417. https://doi.org/10.1126/sciadv.adj2417.
6. Levy AM, Saling MM, Anderson JFI. Cognitive symptoms are not associated with cognitive performance in Post-Acute mTBI. Arch Clin Neuropsychol. 2025;40(1):63–74. https://doi.org/10.1093/arclin/acae060.
7. Herman AB, Tsitsipatis D, Gorospe M. Integrated LncRNA function upon genomic and epigenomic regulation. Mol Cell. 2022;82(12):2252–66. https://doi.org/10.1016/j.molcel.2022.05.027.
8. Zhang N, Ding C, Zuo Y, Peng Y, Zuo L. N6-methyladenosine and neurological diseases. Mol Neurobiol. 2022;59(3):1925–37. https://doi.org/10.1007/s12035-022-02739-0.
9. Wu X, Liu H, Wang J, et al. The m6A methyltransferase METTL3 drives neuroinflammation and neurotoxicity through stabilizing BATF mRNA in microglia. Cell Death Differ. 2025;32(1):100–17. https://doi.org/10.1038/s41418-024-01329-y.
10. Xiao M, Wang X, Xiao E, Ming Q. Overexpression of FTO alleviates traumatic brain injury induced posttraumatic epilepsy by upregulating NR4A2 expression via m6A demethylation. Funct Integr Genomics. 2025;25(1):17. Published 2025 Jan 18. https://doi.org/10.1007/s10142-024-01522-9
11. Zhang M, Hamblin MH, Yin KJ. Long non-coding RNAs mediate cerebral vascular pathologies after CNS injuries. Neurochem Int. 2021;148:105102.
12. Chodurska B, Kunej T. Long non-coding RNAs in humans: classification, genomic organization and function. Non-coding RNA Res. 2025;11:313–27.
13. Yan L, Han X, Zhang M, et al. Integrative analysis of TBI data reveals Lgmn as a key player in immune cell-mediated ferroptosis. BMC Genomics. 2023;24(1):747. https://doi.org/10.1186/s12864-023-09842-z. Published 2023 Dec 6.
14. Chen B, Yuan C, Guo T, Liu J, Yang B, Lu Z. Molecular mechanism of m6A methylation modification genes METTL3 and FTO in regulating heat stress in sheep. Int J Mol Sci 2023, 24(15).
15. Zhang J, Wei J, Sun R, Sheng H, Yin K, Pan Y, Jimenez R, Chen S, Cui XL, Zou Z, et al. A LncRNA from the FTO locus acts as a suppressor of the m(6)A writer complex and p53 tumor suppression signaling. Mol Cell. 2023;83(15):2692–e27082697.
16. Liu Y, Shi M, He X et al. LncRNA-PACERR induces pro-tumour macrophages via interacting with miR-671-3p and m6A-reader IGF2BP2 in pancreatic ductal adenocarcinoma. *J Hematol Oncol*. 2022;15(1):52. Published 2022 May 7. https://doi.org/10.1186/s13045-022-01272-w
17. Ma C, Gou C, Sun S, et al. Unraveling the molecular complexity: Wtap/Ythdf1 and Lcn2 in novel traumatic brain injury secondary injury mechanisms. Cell Biol Toxicol. 2024;40(1):65. https://doi.org/10.1007/s10565-024-09909-x. Published 2024 Aug 7.
18. Lu Z, Huang K. Protective effect of Silencing LncRNA HCP5 against brain injury after intracerebral hemorrhage by targeting miR-195-5p. BMC Neurosci. 2025;26(1):2. https://doi.org/10.1186/s12868-024-00923-7. Published 2025 Jan 8.
19. Yu J, Zhang Y, Ma H et al. Epitranscriptomic profiling of N6-methyladenosine-related RNA methylation in rat cerebral cortex following traumatic brain injury. Mol Brain. 2020;13(1):11. Published 2020 Jan 28. https://doi.org/10.1186/s13041-020-0554-0
20. Xue Y, Zhang Y, Wu Y, Zhao T. Activation of GPER-1 attenuates traumatic brain Injury-Induced neurological impairments in mice. Mol Neurobiol. 2024;61(8):5614–27. https://doi.org/10.1007/s12035-024-03919-w.
21. Dierks D, Garcia-Campos MA, Uzonyi A, Safra M, Edelheit S, Rossi A, Sideri T, Varier RA, Brandis A, Stelzer Y, et al. Multiplexed profiling facilitates robust m6A quantification at site, gene and sample resolution. Nat Methods. 2021;18(9):1060–7.
22. Qiu Y, Man C, Zhu L, et al. R-loops' m6A modification and its roles in cancers. Mol Cancer. 2024;23(1):232. https://doi.org/10.1186/s12943-024-02148-y. Published 2024 Oct 18.
23. Wang D, Zheng T, Zhou S, et al. Promoting axon regeneration by inhibiting RNA N6-methyladenosine demethylase ALKBH5. Elife. 2023;12:e85309. https://doi.org/10.7554/eLife.85309. Published 2023 Aug 3.
24. Xu W, Li J, He C, et al. METTL3 regulates heterochromatin in mouse embryonic stem cells. Nature. 2021;591(7849):317–21. https://doi.org/10.1038/s41586-021-03210-1.
25. Wade S, Hadj-Moussa H, Storey KB. mRNA m(6) A methylation in wood frog brain is maintained during freezing and anoxia. J Exp Zool Ecol Integr Physiol. 2023;339(3):325–34.
26. Xin Y, He Q, Liang H, Zhang K, Guo J, Zhong Q, Chen D, Li J, Liu Y, Chen S. m(6) A epitranscriptomic modification regulates neural progenitor-to-glial cell transition in the retina. Elife 2022, 11.
27. Yu J, Zhang Y, Ma H et al. Epitranscriptomic profiling of N6-methyladenosine-related RNA methylation in rat cerebral cortex following traumatic brain injury. *Mol Brain*. 2020;13(1):11. Published 2020 Jan 28. https://doi.org/10.1186/s13041-020-0554-0
28. Song M, Yi F, Zeng F, et al. USP18 stabilized FTO protein to activate mitophagy in ischemic stroke through repressing m6A modification of SIRT6. Mol Neurobiol. 2024;61(9):6658–74. https://doi.org/10.1007/s12035-024-04001-1.
29. Lv D, Yang K, Rich JN. Growth factor receptor signaling induces mitophagy through epitranscriptomic regulation. Autophagy. 2023;19(3):1034–5.
30. Luo XJ, Lu YX, Wang Y, et al. M6A-modified LncRNA FAM83H-AS1 promotes colorectal cancer progression through PTBP1. Cancer Lett. 2024;598:217085. https://doi.org/10.1016/j.canlet.2024.217085.
31. Ghosh S, Saha A, Singh R, et al. Long noncoding RNA VLDLR-AS1 levels in serum correlate with Combat-Related chronic mild traumatic brain injury and depression symptoms in US veterans. Int J Mol Sci. 2024;25(3):1473. https://doi.org/10.3390/ijms25031473.
32. Patel NA, Moss LD, Lee JY, Tajiri N, Acosta SA, Borlongan CV. Long noncoding RNA MALAT1 in exosomes drives regenerative function and modulates inflammation-linked networks following traumatic brain injury. J Neuroinflammation. 2018;15(1):204. https://doi.org/10.1186/s12974-018-1240-3.
33. Chen Y, Zhang Y, Wang Y, et al. LncRNA H19 knockdown promotes neuropathologic and functional recovery via the Nrf2/HO-1 axis after traumatic brain injury. CNS Neurosci Ther. 2024;30(4):e14870. https://doi.org/10.1111/cns.14870.
34. Zhao Y, Wang H, Yang Y, et al. Silencing long non-coding RNA zinc finger antisense 1 restricts secondary cerebral edema and neuron injuries after traumatic brain injury. Brain Res Bull. 2021;170:1–9. https://doi.org/10.1016/j.brainresbull.2021.02.002.
35. Ji RR, Chamessian A, Zhang YQ. Pain regulation by non-neuronal cells and inflammation. Science. 2016;354(6312):572–7. https://doi.org/10.1126/science.aaf8924.
36. Tao R, Stöhr O, Wang C, Qiu W, Copps KD, White MF. Hepatic follistatin increases basal metabolic rate and attenuates diet-induced obesity during hepatic insulin resistance. Mol Metab. 2023;71:101703.
37. Xu J, Su Z, Ding Q, et al. Inhibition of proliferation by knockdown of transmembrane (TMEM) 168 in glioblastoma cells via suppression of Wnt/β-Catenin pathway. Oncol Res. 2019;27(7):819–26. https://doi.org/10.3727/096504018X15478559215014.

Publisher's note